**Atmospheric
Chemistry
and Physics
Discussions**

Dependence of SOA oxidation on organic aerosol mass concentration and OH exposure: experimental PAM chamber studies

E. Kang[1,3], D. W. Toohey[2], and W. H. Brune[1]

[1]Department of Meteorology, Pennsylvania State University, University Park, PA 16802, USA
[2]Department of Atmospheric and Oceanic Sciences, University of Colorado, Boulder, CO 80309-0311, USA
[3]Department of Earth and Environmental Science, Korea University, Seoul, 136-701, Korea

Correspondence to: E. Kang (ekang@korea.ac.kr)

ACPD

10, 24053–24089, 2010

SOA oxidation PAM chamber studies

E. Kang et al.

Title Page

Abstract	Introduction
Conclusions	References
Tables	Figures

◄◄ ►►

◄ ►

Back Close

Full Screen / Esc

Printer-friendly Version

Interactive Discussion

Abstract

The oxidation of secondary organic aerosol (SOA) is studied with mass spectra analysis of SOA formed in a Potential Aerosol Mass (PAM) chamber, a small flow-through photo-oxidation chamber with extremely high OH and ozone levels. Oxidation for a few minutes in the PAM chamber is equivalent to days to weeks in the atmosphere. The mass spectra were measured with a Quadrupole Aerosol Mass Spectrometer (Q-AMS) for SOA formed from oxidation of α-pinene, m-xylene, p-xylene, and a mixture of the three. The organic mass fraction of m/z 44 (CO_2^+) and m/z 43 (mainly $C_2H_3O^+$), named f_{44} and f_{43}, respectively, are used as indicators of the degree of organic aerosol (OA) oxidation that occurs as the OA mass concentration or the OH exposure are varied. The degree of oxidation is sensitive to both. For a fixed OH exposure, the degree of oxidation initially decreases rapidly and then more slowly as the OA mass concentration increases. For fixed initial precursor VOC amounts, the degree of oxidation increases linearly with OH exposure, with linear f_{44} increase and f_{43} decrease. The degree of oxidation seen in this study is similar to that seen in large environmental chambers for the least oxidized OA and similar to the atmosphere for the most oxidized OA. These results, while sensitive to the determination of f_{44} and f_{43}, provide evidence that characteristics of atmospheric OA oxidation can be generated in a PAM chamber. For all measurements in this study, the sum of f_{44} and f_{43} is 0.25 ± 0.03, so that the slope of a linear regression is approximately -1 on an f_{44} vs. f_{43} plot. This constancy of the sum suggests that these ions are complete proxies for organic mass in the OA studied.

1 Introduction

Organic aerosol (OA) is a significant fraction of the total atmospheric aerosol (Kanakidou et al., 2005) and, as a result, affects both climate change by changing Earth's radiative balance (Hoyle et al., 2009; Myhre et al., 2009) and human health by degrading the cardiovascular system (Jang et al., 2006; Baltensperger et al., 2008). A significant

fraction of OA is secondary organic aerosol (SOA), which is formed when atmospheric oxidants such as the hydroxyl radical (OH) and ozone (O_3) react with volatile organic compounds (VOCs) to form lower volatility organics. These VOCs are numerous and include biogenic terpenes, anthropogenic alkenes, aromatics, and long-chain alkenes. Because of the importance of SOA to both climate and human health, SOA has become a focus of intense laboratory, theoretical, and observational research (Nel, 2005; Forster et al., 2007; Jimenez et al., 2009; Ng et al., 2010).

Understanding the atmospheric evolution of SOA is as important as understanding the sources of the precursor VOCs because as organic particles age and become more oxidized, they become more hygroscopic and serve as cloud condensation nuclei (Zhang et al., 2005; Alfarra et al., 2006; Lanz et al., 2007; Ulbrich et al., 2009; Jimenez et al., 2009). With further oxidation, the semi-volatile and low-volatility organics become fragmented into smaller more volatile molecules, the ultimate result being carbon dioxide (CO_2). SOA and primary organic aerosol (POA) can be hydrocarbon-like OA (HOA), semi-volatile oxygenated OA (SV-OOA), or low-volatility oxygenated OA (LV-OOA) with the degree of oxidation determined in part by the amount of time the OA are exposed to oxidants. The results of this aging process have been observed in both the atmosphere (Lanz et al., 2007; Zhang et al., 2007; Ng et al., 2010) and the laboratory (Jimenez et al., 2009; Shilling et al., 2009; George and Abbatt, 2010).

The evolution of SOA appears to be complicated. Unlike sulfate that remains in the particle phase, the organic constituents that compose OA are semi-volatile and continually partition between the particle and gas phases. The aging process can cause the shift in the gas and particle partitioning equilibrium by dilution with fresh air, the further oxidation of the gaseous product, heterogeneous oxidation of the organic layer in the particle, and the reactions that lead to oligomer formation (Donahue et al., 2006; Rudich et al., 2007). Oxidants such as hydroxyl (OH), ozone (O_3), hydroperoxyl (HO_2), organic peroxyl (RO_2), nitric oxide (NO), and nitrogen dioxide (NO_2) affect the yields and identity of the reaction products. In some situations, organics in OA may be directly decomposed by the ultraviolet light (UV) (Kroll et al., 2006; Surratt et al.,

SOA oxidation PAM chamber studies

E. Kang et al.

2006; Lambe et al., 2007; Warren et al., 2008). New modeling frameworks are being developed to account for these changes in OA with atmospheric oxidation (Dzepina et al., 2009; Jimenez et al., 2009), but the uncertainties and unknowns in OA oxidation are large. Measured OA can greatly exceed the model calculated OA by a factor of 4

5   to 100 (Volkamer et al., 2006). The cause of this discrepancy is currently unknown but may result from unmeasured VOCs, unknown oxidation processes, or measurement errors.

To complicate this problem further, controlled laboratory chambers and flow tubes offer only imperfect simulations of OA atmospheric oxidation. Problems include using

10   VOCs amounts well above atmospheric levels, potentially interactive walls (Matsunaga and Ziemann, 2010), and levels of oxidants or oxidant precursors that are significantly larger than those in the atmosphere. A key test is to compare the chemical composition of the OA produced in these chambers with that observed in the atmosphere. For large environmental chambers, the chemical composition of OA is much more hydrocarbon-

15   like than the OA observed in the atmosphere (Bahreini et al., 2005; Alfarra et al., 2006; Zhang et al., 2006; Shilling et al., 2009; Ng et al., 2010), probably because the aging is much less than in the atmosphere. It has been possible to overcome this limitation by creating highly oxidative environments in small chambers and flow tubes (Jimenez et al., 2009; Kroll et al., 2009; George and Abbatt, 2010), but the resulting chemical

20   composition has too much SV-OOA for the observed amounts of LV-OOA (Ng et al., 2010). These conclusions are based on only a few laboratory studies.

In this paper, we present the results of OA oxidation studies conducted in the highly oxidizing environment of a Potential Aerosol Mass chamber (Kang et al., 2007). In a previous manuscript, we introduced the concept of Potential Aerosol Mass (PAM),

25   which is defined as the maximum aerosol mass that the oxidation of precursor gases produces, and presented the results of extensive tests of the chamber performance and the OA yields of several atmospherically relevant VOCs (Kang et al., 2007). A Tapered Element Oscillation Microbalance (TEOM) was used to measure the OA mass in those studies. During those experiments, we also sampled the OA chemical composi-

tion from the PAM chamber using a Quadrupole-Aerosol Mass Spectrometer (Q-AMS). In this study, we use mass spectra taken with the Q-AMS to examine the chemical characteristics of OA as a function of the OA mass concentration and the OH exposure and to compare these results to those from other recent laboratory studies.

2 Experimental method

These studies used a flow-through PAM chamber in which extreme levels of OH and O_3 were generated (Fig. 1). The outflow of this chamber was sampled with a TEOM monitor 1400 AB (The Thermo Scientific, Franklin, MA), a Q-AMS (Aerodyne Research, Inc., Bellerica, MA), and miscellaneous gas sampling instruments. Whereas our previous study focused on the TEOM results, this study focuses on the Q-AMS data. Additional monitoring of the refractive index of the particles using the Ultra-high Sensitivity Aerosol Spectrometer (UHSAS, ParticleMetrics, Inc., Boulder, CO) will not be discussed here.

The mass spectrum of OA enables the determination of the degree of oxidation that the OA has undergone. HOA is identified by the mass to charge ratios (*m/z*) 41, 43, 55, 57, 69, 71 and OOA is mainly identified by *m/z* 43 and 44. SV-OOA is characterized as a relatively less aged aerosol with more volatile organic compounds. Thus ambient SV-OOA is often highly correlated with semi-volatile species like ammonium nitrate and ammonium chloride, has a low ratio of oxygen to carbon (O:C), and has more *m/z* 43 than *m/z* 44 contributions to the OA mass concentration. In contrast, LV-OOA has more *m/z* 44 than *m/z* 43. SV-OOA and LV-OOA are not uniquely defined but form a continuum of the degree of oxidation. While Principle Component Analysis provides a more rigorous characterization of atmospheric OA, the use of *m/z* 43 and *m/z* 44 are sufficient to track the degree of oxidation in single-precursor laboratory experiments such as ours (e.g., Shilling et al., 2009; Ng et al., 2010).

The contributions of the mass concentrations at *m/z* 43 and *m/z* 44 to OA mass concentration, called f_{43} and f_{44} (Ng et al., 2010), have been used to indicate the degree of OA oxidation, along with the O:C ratio and the overall mass spectrum (Lanz et al.,

2007; Aiken et al., 2008; Jimenez et al., 2009). For the comparison of various OA aging processes in the atmosphere and laboratory studies, a generalized clear definition of the contribution of the mass concentrations at m/z 43 and m/z 44 to OA mass concentrations is required. For this study, f_{43} and f_{44} are defined as the mass concentrations at m/z 43 and m/z 44 divided by the OA mass concentrations as determined from Q-AMS fragmentation tables (Allan et al., 2004) that are modified to attribute the total observed mass to organics.

2.1 PAM chamber description

The PAM chamber and its operation are described in detail in Kang et al. (2007), so only a brief description is presented here (Fig. 1). This version of the PAM chamber was a continuous flow 19 L cylinder (diameter 20 cm, length 60 cm) made of Teflon FEP film (0.5 mm thick) and suspended in a sealed housing. Two ozone producing UV grid lamps (BHK Inc., Ontario, CA) that mainly produced 185 nm and 254 nm light were mounted on a wall of the housing. The volume inside of the housing surrounding the Teflon chamber was purged with N_2 gas to prevent gas impurities from diffusing through the Teflon into the chamber air and to prevent ozone formation in the space between the Teflon chamber and housing. The sample air was continuously added into the PAM chamber and removed through a large exhaust hose at the bottom of the PAM chamber. Aerosol particles, gases, relative humidity, pressure, and temperature were sampled from the bottom of the PAM chamber.

To distribute the air flow evenly into the chamber and to reduce losses on the wall surfaces, the sample air was added through tubes that had many tiny drilled holes and spiraled out from a central tube. Approximately 60% of the flow was sampled by the instrument inlet in the center of the bottom plate, while the rest exited the chamber through a ring that surrounded the sampling inlet. Possible wall effects in the PAM chamber were examined by adding SO_2, turning on the UV lights to produce OH, and then measuring the SO_2 decrease and the sulfate mass increase. Sulfate aerosol is known to be rapidly lost to wall surfaces, but the conversion of SO_2 to sulfate in the

chamber agreed with theory to within 10%, indicating that wall loss had little effect on the sampled air.

2.2 Experimental conditions

The SOA formation experiments were carried out using photo-oxidation of three precursor VOCs: α-pinene, m-xylene and p-xylene. The PAM chamber was continuously flushed with humidified and purified zero air overnight before experiments the next day. In addition, a humidified zero air flow was frequently irradiated by UV lamps to clean up the chamber and to test for particle formation, which would indicate problems with wall interactions or impure zero air. The flow rate in the chamber was $5\,L\,min^{-1}$, which produced a mean residence time of $240\pm36\,s$. VOC gas mixtures, prepared in ultra zero N_2 gas, were combined with humidified zero air prior to the PAM chamber inlet and then added into the chamber. The stated purities of parent VOCs and N_2 gas are as follows: α-pinene (Fluka, 99.0%), m-xylene (Fluka, 99.5%), p-xylene (Fluka, 99.5%), and N_2 (99.999% pure, <0.5 ppm THC, GTS). The preparation method was described previously (Kang et al., 2007).

The oxidants O_3, OH, and HO_2 were generated in the PAM chamber by turning on the UV lamps. O_3 was kept constant at 9 ppmv, while OH and HO_2 were varied from 60 pptv to 500 pptv and 0.45 ppbv to 4 ppbv, respectively, by varying the relative humidity. The pressure of the chamber was ambient, approximately 960 hPa. The amount of OH in the chamber was calibrated as a function of relative humidity by sampling from the chamber with the Ground-based Tropospheric Hydrogen Oxides Sensor (GTHOS) and by measuring the decrease in SO_2 as OH was added (Root, 2007; Kang et al., 2007). The relationship between OH and relative humidity is given by OH(pptv)=$9.3643\times$RH(%)+34.643, r^2=0.99. The relative humidity range was 3 to 45%. The absolute uncertainty of this calibration is ±32%, 2σ uncertainty (Faloona et al., 2004). The photo-oxidation and particle formation was initiated and terminated by turning on and off the UV lamp.

SOA oxidation PAM chamber studies

E. Kang et al.

Title Page

Abstract	Introduction
Conclusions	References
Tables	Figures

◄ | ►I

◄ | ►

Back | Close

Full Screen / Esc

Printer-friendly Version

Interactive Discussion

OH exposure, which is OH concentration (molecules cm^{-3}) integrated over the time in the PAM chamber, determines how fast the precursor VOCs and their products are oxidized. The rates for reactions between OH and VOCs are large; for instance $k_{\text{OH}+\alpha}$-pinene$=5\times10^{-11}$ molecules^{-1} cm^3 s^{-1}, $k_{\text{OH}+m}$-xylene$=2.44\times10^{-11}$ molecules^{-1} cm^3 s^{-1}, and $k_{\text{OH}+p}$-xylene$=1.5\times10^{-11}$ molecules^{-1} cm^3 s^{-1} at 300 K (NIST Chemical Kinetics Database, Version 7.0, 2000). For even the largest VOC amount and smallest OH amount, VOCs were oxidized and OH returned to a stable value within the first 150 s in the chamber, with OH recovering faster for α-pinene than for the xylenes. This modeling result is confirmed by gas chromatographic measurements that show no VOCs remained at the bottom of the chamber for all experiments. Photochemical modeling also shows that OH exposure was reduced by the presence of the high VOC amounts, by as much as 40% in the worst case. These modeling calculations have been used to correct the OH exposure determined from relative humidity. For experiments with various VOC amounts and fixed OH, OH exposures decreased with increasing VOC amounts, decreasing 20% for α-pinene, 33% for m-xylene, and 23% for p-xylene. An OH exposure of 10^{12} molecules cm^{-3} s in the PAM chamber is equivalent to an ambient exposure time of ~5 days (for a typical diurnally averaged OH concentration of 1.5×10^6 molecules cm^{-3}).

We performed two different types of experiments. The first examined the SOA oxidation as a function of precursor VOC amount and the second examined the SOA oxidation as a function of OH exposure. The detailed experimental conditions are presented in Table 1. All experiments were performed at a constant temperature of 25 °C with neither seed particles nor NO$_x$. For experiments with various precursor VOC amounts, O$_3$ and final OH amount were kept constant at 9 ppmv and 260 pptv, respectively. Relative humidity was also controlled in the 23 to 25% range and temperature was kept constant at 25±1 °C. For experiments with various OH amounts, O$_3$ was kept constant at 9 ppmv while OH was varied in the range of 60 pptv to 500 pptv by changing the relative humidity over the range of 3 to 45%.

2.3 Instrumentation

Both gases and particles were measured at the bottom of the PAM chamber (Fig. 1). O_3 was continuously monitored with the Model 8810 Ozone Analyzer (Monitor Labs Inc.), NO/NO_x with the 42C Trace level $NO–NO_2–NO_y$ analyzer (Thermo Environ-
5 mental Instruments), and relative humidity and temperature with a HUMICAP HMP 45 A/D (Vaisala). Initial and final VOC amounts were measured by the 8610C Gas Chromatography-Flame Ionization Detector (GC-FID) (SRI Instruments, Torrence, CA). Aerosol mass concentration was continuously measured by the TEOM. The TEOM temperature was set to 30˚C and the air stream was not dried in order to avoid the
10 loss of semi-volatile species by evaporation. Aerosol mass concentration was calculated from 2-min averages of the TEOM raw frequency. The detailed TEOM setup was described previously (Kang et al., 2007).

The chemical composition of OA was measured by Q-AMS. In this study, we use the mass spectra of total particles regardless of size from the Q-AMS operated in the
15 MS-mode. Detailed operational information of Q-AMS can be found elsewhere (Jayne et al., 2000; Canagaratna et al., 2007) and only brief description is given here. The Q-AMS can measure size-resolved chemical composition of aerosol in the atmosphere by alternating between two modes, called mass spectrum (MS) and particle time of flight (pTOF). In the MS mode, the quadrupole is scanned from m/z 1 to 300 to ob-
20 tain a volume (or mass)-averaged MS of the sampled aerosol. In the pTOF mode it scans a pre-selected number of ion fragment masses from a chopped particle beam. Because the entire mass spectra scan cannot be completed for single particles due to the short duty cycle in pTOF mode, Q-AMS provides limited single particle information. In this study, we are primarily interested in the ensemble mass spectrum of the
25 sampled aerosol. Therefore, the Q-AMS is adequate for a controlled laboratory study involving purified air and a single VOC or a simple mixture of VOCs (Drewnick et al., 2005; Canagaratna et al., 2007).

3 Results and discussion

3.1 Characteristics of SOA generated in a highly oxidizing environment

3.1.1 Mass spectra of SOA

Examples of mass spectra of SOA formed in the PAM chamber for three VOCs at a constant OH are shown in Fig. 2. Overall, four dominant peaks were observed at *m/z* 18, 28, 43, and 44. Fragments at higher molecular weights were observed (such as *m/z* 55, 57, 67, and or higher *m/z*) but these individual peaks were smaller than the four dominant ones. The relatively high contribution of *m/z*>50, for instance *m/z* 57, 67, and 69, are commonly found for HOA and consist of unsaturated hydrocarbons, unsaturated alcohols, unsaturated carbonyl groups, or freshly formed SOA from the urban plume or diesel exhaust. The dominance of *m/z* 43 and 44 observed in these experiments is a characteristic of OOA that is commonly observed in rural or remote atmospheres, hours-to-days downwind on SOA sources (Bahreini et al., 2005; Zhang et al., 2005; Ng et al., 2010). It is not surprising that the SOA in the PAM chamber resemble OOA, since the smallest OH exposure in the PAM chamber is 1.8×10^{11} cm^{-3} s, equivalent to about 1.4 days in the atmosphere, assuming an average OH concentration of 1.5×10^6 cm^{-3}. In the following discussions, the mass spectrum peaks at *m/z* 43 and *m/z* 44 will be used as indicators of the relative oxidation of the SOA as the VOC type and amount or the OH exposure are varied.

3.1.2 The determination of OA mass concentration for this study

The SOA mass concentrations generated in the PAM chamber were directly measured by TEOM and compared with the OA mass concentrations that were calculated from the AMS mass spectrum analysis. The calculation of the OA mass concentration depends on assumptions about which mass peaks contribute to the OAs.

The fragmentation table reported in Allan et al. (2004) was the basis for the calculation of OA mass concentration reported here. This table was modified to account for peaks that, in measurements of ambient aerosols, are dominated by air or by non-organic particulate compounds, but in these experiments with high OA mass concentrations correlate strongly with organic peaks, such as m/z 43 and 44. Thus, signals from fragments at m/z 14, 28, 31, 33, 34, 36, 39, 40, 46, and 47 are included in the calculation of OA mass concentration, excluding backgrounds measured in the absence of particles. In addition, small adjustments have been made to the Allan et al. (2004) relationships at m/z 16, 17, 18, 19, 30, and 48 to account for correlations of these peaks with organic peaks (e.g., and m/z 29, 44, and 62) that were observed for each set of experiments (Table 2). In this manner, the fragmentation table correctly attributed >99% of the OA mass concentration, with negligible attribution to other common ambient species such as sulfate, nitrate, and ammonium.

Because significant particulate signals were observed at m/z 28 (presumably due to CO^+ and $C_2H_2^+$), m/z 32 was chosen for the air beam reference for normalization to the AMS-standard pre- and post-experiment calibrations that employed ammonium nitrate aerosols. The signals at m/z 32 did not vary with OA mass concentration, indicating that this mass was suitable for tracking any drift in sensitivity or tune of the quadrupole mass analyzer over the course of a series of experimental runs. A sample set of changes to the Allan et al. (2004) fragmentation table is shown in Table 2. The total OA mass concentration calculated here was about 25% greater than values obtained using the Allan et al. (2004) fragmentation table, due mostly to adjustments in m/z 18 and m/z 28 and inclusion of m/z 14, 39, and 40.

It is important to note here that in these experiments, for which expected products are pure organics and signals are much larger than in ambient measurements, it is relatively straightforward to account for the OA mass concentration. It is more difficult to account for OA mass concentration in ambient measurements. Consequently, it is reasonable to compare values of f_{43} and f_{44} from laboratory experiments (e.g., flow tubes or environmental chambers), but comparisons to ambient measurements (e.g., Ng et

al., 2010) are more complicated. It is likely that f_{43} and f_{44} values calculated with modified fragmentation tables that account for all the OA mass concentration as described above will be systematically smaller than values calculated for ambient aerosols with standard fragmentation tables.

The OA mass concentration calculated from this AMS spectrum analysis is in a good agreement with TEOM-measured aerosol mass concentrations with a slope of 0.90 and r^2 of 0.98 (Fig. 3). For these laboratory studies in which all the aerosol mass comes from the oxidation of VOCs, the OA mass concentration, as determined by the AMS analysis, should be the same as the total aerosol mass concentration, as determined by the TEOM. An AMS underestimation of the OA mass concentration could occur for three reasons: (1) the limited transmission of the AMS lens about 50~1500 nm in size, (2) evaporation of volatile components such as water and some light organics, and (3) potential particle bounce which results in less than 100% particle collection efficiency (Allan et al., 2004). The fact that AMS particulate masses within 10% of the TEOM mass tells us that the evaporative losses inside the AMS must be small and the collection efficiency must be close to 1. When the uncertainties in the TEOM measurement and the AMS analysis are considered, the absolute uncertainty in the AMS OA mass concentration is estimated to be 32% at the 2σ confidence level.

3.1.3 Oxidation indicators f_{44} and f_{43}

The fractions f_{44} and f_{43} were calculated as the ratios of the mass concentrations at m/z 44 and m/z 43 to the OA mass concentrations. The OA mass concentration was obtained by the modified fragmentation table as described above. Depending on the assignment of m/z peaks or fractions of m/z peaks as organics, the calculated OA mass concentrations, thus f_{44} and f_{43}, differs by as much as 15–25%. If f_{44} and f_{43} are to be used as generalized oxidation indicators and for comparing oxidation processes in different laboratory and field studies, then the publication of each study should contain a description or reference of the determination of OA mass concentrations in order to make the comparisons among published studies valid.

3.2 Effect of OA mass concentration on the SOA oxidation

The dependence of SOA oxidation on OA mass concentration was studied by varying the amounts of three VOCs, α-pinene, m-xylene and p-xylene. O_3 was kept constant at 9 ppmv and the final OH amount was fixed to 259 pptv, resulting in the OH exposures in Table 1. The amount of α-pinene was varied from 7 to 79 ppbv, m-xylene from 87 to 426 ppbv, and p-xylene from 141 to 371 ppbv (Table 1). These mixing ratios are greater than those found in the atmosphere, although the smallest α-pinene amounts are comparable to total VOC amounts in the atmosphere.

As VOC amounts increased, the measured OA mass concentration increased (Fig. 4a). The photo-oxidation of α-pinene generated more OA mass than m-xylene because the OA yield is greater for α-pinene than m-xylene in a PAM chamber (Kang et al., 2007). OA in the PAM chamber was formed from the direct photo-oxidation of VOCs without seed particles or POA, thus the OA mass concentration was directly proportional to the VOC amount. As can be seen by the upward curvature of all plots in Fig. 4a, the OA yield increased with VOC amounts, indicating an increase in the partitioning in the condensed phase with increasing OA mass concentration (Odum et al., 1996; Donahue et al., 2006).

The OA mass yields are greatly different for α-pinene and xylenes (m-xylene and p-xylene), but the fractions of m/z 43 and m/z 44 to the total OA mass concentration, f_{43} and f_{44}, have almost the same dependence on the OA mass concentration (Fig. 4b,c). The ratio of f_{44} to f_{43} of xylenes was about 10–20% smaller than that of α-pinene, but the decrease in f_{44}/f_{43} as the OA mass concentration increases is similar (Fig. 4b), with the difference that the OA mass concentration at which f_{44}/f_{43} equals one is much less for xylenes. These results show that the amount of oxidation depends strongly on the OA mass concentration, especially for low OA mass concentrations. There is a rapid decrease in the ratio with increasing OA below 50 μg m^{-3}, leveling off at higher OA mass concentrations. For the lowest α-pinene mixing ratio, 7 ppbv, f_{44}/f_{43} is 3.2 and f_{44} is 0.19, consistent with aged atmospheric OA (Ng et al., 2010, Fig. 5).

As the OA mass concentration increased, f_{43} increased and both f_{44} and atomic oxygen-to-carbon (O:C) ratios decreased (Fig. 4c). The O:C ratio was calculated using the approximate correlation equation, O/C atomic ratio=$(0.0382\pm0.0005)\times(m/z\ 44/\ OA\ (in\ \%))+(0.0794\pm0.0070)$, from Aiken et al. (2008). The O:C ratio for α-pinene in this study decreased from 0.8 to 0.5 for a range of OA mass concentrations of 11.8 to 216 μg m^{-3}. For m-xylene and p-xylene, the ratio decreased from 0.7 to 0.4 for a range of OA mass concentrations within 16 and 271 μg m^{-3}. These f_{44} and O:C ratios are comparable to those observed in the atmosphere, where O:C ratios vary widely from 0.2 to 1.0 (Aiken et al., 2008; Jimenez et al., 2009; Ng et al., 2010). On the other hand, O:C ratios observed in environmental chambers and some flow tubes are less than 0.5 (Aiken et al., 2008; George and Abbatt, 2010; Ng et al., 2010), quite different from the atmosphere and from this study.

The decrease of f_{44} and increase of f_{43} with increasing OA mass concentration is significant. The ratio of f_{44} to f_{43} shows similar behavior. One possible explanation for this behavior is that more volatile and less oxidized organics are able to condense as the OA mass concentration increases (Donahue et al., 2006). As a result, an increasing fraction of the OA is less oxidized, thus shifting f_{43} up and f_{44} down. The non-linear behavior of f_{44} and f_{43} as a function of OA mass concentration (Fig. 4b,c) must then be related to the volatility of the semi-volatile organics that are condensing. The cross-over point (i.e., where f_{44} and f_{43} are equal) for m-xylene and p-xylene is at a lower OA mass concentration than α-pinene, suggesting that the organics in the xylenes OA are less volatile and more oxidized than those in the α-pinene OA, a conclusion also reached by Ng et al. (2010).

The behavior of f_{44} as a function of OA mass concentration observed in this study is similar to the compilation of photo-oxidation and ozonolysis experiments in Ng et al. (2010). The difference between this study and the previous ones is that f_{44} for this study is about twice as large as that measured in most studies at low OA mass concentrations and in all studies at mass concentrations greater than 50 μg m^{-3}. Our study may get this result because the PAM chamber samples the OH high-exposure

Title Page

Abstract | Introduction

Conclusions | References

Tables | Figures

◄ | ►

◄ | ►

Back | Close

Full Screen / Esc

Printer-friendly Version

Interactive Discussion

region of f_{44} and f_{43} values.

3.3 Effect of OH exposure on the SOA oxidation

The effect of OH exposure on the SOA formation and oxidation was studied with different levels of OH exposure in the PAM chamber. Initial VOCs concentrations were
5   35 ppbv of α-pinene, 150 ppbv of m-xylene, 133 ppbv of p-xylene, and a mixture of 37 ppbv of α-pinene, 46 ppbv of m-xylene and 47 ppbv of p-xylene. The OH exposure was changed by changing the relative humidity and added VOC amounts. The effect of relative humidity itself on the SOA was found to be negligible for these precursor VOC gases (Kang et al., 2007). By changing the relative humidity over the range of
10   3 to 45%, the OH was changed from 63 pptv to 480 pptv, and the OH exposure was changed from 1.8×10^{11} cm^{-3} s to 2.4×10^{12} cm^{-3} s.

The OH exposure affected the OA mass concentration as well as the chemical characteristics (Fig. 5a). In a simple conceptual model of OA oxidation, the OA mass concentration builds as the OH exposure begins and VOCs are oxidized to less volatile
15   organics. With further oxidation, fragmentation can occur, resulting in more volatile organics and loss of OA mass concentration. Oxidation pathways seemed to be divided to fragmentation and oligomerization (Gross et al., 2006; Jimenez et al., 2009), but in this study oligomerization was not the dominant process, which is similar to the conclusion of Heald et al. (2010).
20   For these studies, the OA mass concentration decreased for all OH exposures. The OA mass concentration decrease, the increase in f_{44}, and the decrease in f_{43} indicate that as the OA organics became more oxidized and potentially fragmented, they became more volatile and the OA particles lost mass. This phenomenon has also been seen in other studies (Warren et al., 2008; Kroll et al., 2009; George and Abbatt, 2010).
25   The peak in OA mass concentrations must have occurred at an OH exposure less than 3.0×10^{11} cm^{-3} s, because the OA mass concentrations decreased and then leveled off at a lower value for α-pinene, m-xylene, p-xylene, and the mixture. The position of this peak depends on the OA mass concentration because f_{44} and f_{43}, and thus chemical

composition and volatility, do (Fig. 4c). As a result, the peak OA yield was probably not observed in this study. Because OA mass concentrations in the atmosphere are generally far less than those used in this study, the amount of OH exposure needed to achieve the peak OA mass concentration will be even less than that employed here.

The ratio of f_{44} to f_{43} increased linearly as the OH exposure increased for all experiments here (Fig. 5b). The measured range of the ratio of f_{44} to f_{43} was 0.63 to 3.3 for OH exposures of 2.8×10^{11} cm^{-3} s to 2.4×10^{12} cm^{-3} s. The maximum values from large environmental chambers are on the lower end of this measured range; for instance, the ratios of f_{44} to f_{43} were 0.6 for 160 ppbv of α-pinene photo-oxidation from Alfarra et al. (2006) and 0.5 for 186 ppbv of α-pinene ozonolysis from Bahreini et al. (2006). The ratio of f_{44} to f_{43} in rural area in British Columbia, Canada and the Jungfraujoch remote high-alpine locations were observed to be 1.7 (Alfarra et al., 2006). It varied from about 0.4 to more than 4.0 for measurements downwind of Mexico City and in Riverside CA (Ng et al., 2010). Thus, the f_{44}/f_{43} values observed in this study are comparable to those observed in the atmosphere even though the SOA mass concentrations observed in this study are far greater than those observed in the atmosphere.

The changes in f_{44}, f_{43}, and f_{44}/f_{43} are all linear with OH exposure. Linear regressions of f_{44}/f_{43} versus OH exposure (Fig. 5b,c) gave slopes of 4.5×10^{-13} cm^3 s^{-1} for α-pinene, 6.3×10^{-13} cm^3 s^{-1} for m-xylene, 5.3×10^{-13} cm^3 s^{-1} for p-xylene, and 1.2×10^{-12} cm^3 s^{-1} for the mixture, with r^2 values greater than 0.98 for all of them. The linear regressions of f_{44} versus OH exposure gave slopes in the range of 2.5×10^{-14} to 3.9×10^{-14} cm^3 s^{-1}, while the linear regressions of f_{43} versus OH exposure gave slopes in the range of -2.5×10^{-14} to -3.4×10^{-14} cm^3 s^{-1}, respectively. The intercepts of the linear regressions were within 20% of each other for both f_{44} and f_{43}. The fraction of other masses, such as f_{57}, is similarly linear with OH exposure, demonstrating that this behavior applies to all AMS masses, not just m/z 43 and m/z 44.

From these experiments, it is not possible to distinguish between the gas-phase oxidation of semi-volatile organics that are in equilibrium with particle phase and the heterogeneous oxidation of organics on the particle surface. However, if the oxidation

is occurring on the particle surface, then the linearity of f_{44} with OH exposure shows that even these high levels of OH do not occupy so many particle surface sites that the oxidation saturates. This observation provides additional information that the high levels of OH in the PAM chamber can be used to simulate atmospheric oxidation.

Considering the differences in the oxidation pathways for α-pinene and the xylenes, it is noteworthy that f_{44} and f_{43}, as indicators of OA oxidation, behave similarly as a function of OH exposure. This similarity suggests that the evolution of f_{44} and f_{43} are dominated by oxidation of the oliphatic groups attached to the aromatic rings, rather than to oxidation (and breaking) of the aromatic rings, since the latter process would lead to a more complex suite of compounds with differing molecular masses. It is therefore interesting that the behavior of f_{44} and f_{43} for the mixture of α-pinene, m-xylene, and p-xylene is somewhat different from that of the individual precursor VOCs. The oxidation of the mixture occurs at a lower OH exposure, as indicated by the crossover of the f_{44} and f_{43} linear fits and the amount of oxidation appears to be greater, as indicated by f_{44}/f_{43}. Yet at the same time, the OA mass concentration decreases similarly to the xylenes that make up 75% of the mixture. More experiments will be needed to understand these observations.

Additional insight into the OA oxidation can be gained from the behavior of f_{44}, f_{43}, and OA mass concentration during individual experiments using m-xylene photo-oxidation as an example (Fig. 6a). Photo-oxidation in the PAM chamber was initiated by turning on the UV lamps only after the gases were flowing and the VOC was well mixed in the chamber. The lamps produce OH immediately, sometimes with brief spikes according to photochemical models, and the final OH amount was reached as the lamps stabilized and the VOCs reacted away in a few minutes. Each point in Fig. 6 is a minute apart; the first point is the lowest f_{44} value observed in each experiment. The high OH concentrations in the chamber rapidly oxidized the VOCs, resulting in the rapid increase of lower volatility organics that partition between the gas and particle phases. For all OH exposures, the OA mass concentration reached a transient peak in 2–3 min and then decreased to the stable values. This transient peak is not understood, but may

be related to OA non-linear oscillatory nucleation and growth (McGraw and Saunders, 1984) and the competing process of oxidation and evaporation as will be described below. The stable OA mass concentrations are greater for the lower OH exposures while the transient peaks are less. For the highest three OH exposures, the transient

5   peaks are the same, as are the stable values. It is interesting to note how f_{44} and f_{43} behave as the OA go through this transient peak to the stable state.

Initially, f_{44} increased as OH exposure increased even as the OA mass concentration grew. However, after the transient peak occurred and the OA began to evaporate, the amount of oxidation, as indicated by f_{44}, increased only slightly or did not change but

10 it was greater for larger OH exposures. This result suggests that microphysics (e.g., evaporation) and not the oxidation of condensed phase was responsible for the decrease in the OA mass concentration between the transient peak and the stable value. It also suggests that most of the oxidation had already occurred by the time the OA mass concentration had peaked. This behavior provides evidence that the oxidation

15 occurred in the gas-phase, followed by partitioning of the low volatility products between the gas and particle phases. The increase in oxidation degree in all of these experiments is seen in a graph of f_{44} versus f_{43} (Fig. 6b). All data plotted in Fig. 6a fall on a line with a slope of -1.15, and intercept of 0.27, and an r^2 of 0.86. For greater OH exposure, f_{44} is higher and f_{43} is lower, as was already shown in Fig. 5c. Note that

20 even the transient values fall on this line.

It can be difficult to compare the effects of OH exposure from this study to those of other studies primarily because the initial precursor VOC type and concentrations are generally different among the studies. However, if the f_{44} vs. OH exposure linear fit for m-xylene is extrapolated to the OH exposure for the Caltech environmental cham-

25 ber, the line passes through the observed data (Ng et al., 2010, Fig. 8.). George and Abbatt (2010) observed the increase of f_{44} with OH exposure for the mono-dispersed SOA from α-pinene ozonolysis, but the slope was about 1/3 of ours (George and Abbatt, 2010, Fig. 4). Why the OA were more efficiently oxidized in this study compared to theirs is not known. It could be that our study used poly-dispersed OA while theirs

used mono-dispersed OA, which changes the surface to volume ratio. Or it could be that the walls in their flow tube are influencing the partitioning between the gas and particle phases (Matsunaga and Ziemann, 2010), causing the fraction of low-volatility organics to be lower in the particles in their flow tube. It could also be that differences in the aerosol mass spectrometers used in the two studies or in the calculation of f_{44} and f_{43} are responsible for the different results. We come back to this point in the next section.

3.4 Comparison of SOA oxidation with atmospheric values and other laboratory studies

A plot of f_{44} and f_{43} is a good indicator of the degree of SOA oxidation (Ng et al., 2010), as long as differences in the operation of the AMSs and in the calculation of f_{44} and f_{43} are similar for the studies being compared. The results of this study are plotted along with those from atmospheric measurements and other laboratory studies (Fig. 7). All one-minute measurements from this study are plotted, both for studies with varying OA mass concentrations and with varying OH exposures. A linear fit to this study's results in Fig. 7 has a slope of -1.01, an intercept of 0.25, and an r^2 of 0.72. The atmospheric measurements generally fall within the triangular space denoted by the dotted blue lines (Ng et al., 2010). Measurements of m-xylene photo-oxidation in the Caltech environmental chamber are consistent with the measurements from this study and fall just outside of the triangle. Measurements from a high-OH flow tube study at LBNL (Jimenez et al., 2009) have more f_{43} for a given f_{44} than any of the other measurements. Thus, the measurements from this study fall just outside of the triangle for less oxidized OA and inside the triangle for more oxidized OA.

For our study, the sum of f_{43} and f_{44} is 0.25 ± 0.03 for essentially all one-minute measurements, independent of the type of study – varying OA mass concentration or varying OH exposure – and of the precursor gas – α-pinene, m-xylene, p-xylene, and even a mixture of them. That this sum does not change significantly suggests that f_{43} and f_{44} are complete proxies for organic mass in the OA studied.

The slope of points on the f_{44} versus f_{43} plot can be viewed as an indicator for the extent of oxidation of the condensed phase products. In the case of α-pinene, products such as pinonaldehyde, pinonic acid, terpenylic acid, and a $C_{10}H_{16}O_4$ hydroperoxyl compound have been identified in ozonolysis experiments (e.g., Chan et al., 2009). Assuming similar products are produced in the high-OH environment of the PAM chamber, we would expect m/z 43 fragments to represent CH_2CHO and CH_3CO (both C_2H_3O) and m/z 44 to represent CO_2^+ (or –COOH, which would readily form CO_2^+ by electron impact) from parent compounds with molecular weights ranging from 168 g mole^{-1} to 200 g mole^{-1}. On a f_{44} vs. f_{43} plot, fragmentation of a single C_2H_3O group from pinonaldehyde would generate an x-intercept of 0.256, whereas fragmentation of CO_2^+ from pinic acid would result in a y-intercept of 0.238. Products with mixed C_2H_3O and COOH (and CO_2^+) functional groups would produce a mix of m/z 43 and m/z 44 fragments that would lie along a line with a slope of –1.0 on the f_{44} to f_{43} plot. Thus, our results for oxidation of α-pinene in the PAM chamber are consistent with the fragmentation of a single functional group with an increased yield of CO_2^+ (and COOH) groups at the expense of C_2H_3O groups with increased OH exposure.

A similar conclusion can be drawn for the xylenes experiments, although it appears that there is less-than-unit fragmentation into m/z 43 and m/z 44 groups (or that there is a modest yield of a compound that does not form m/z 43 or m/z 44 fragments upon electron impact ionization. Nevertheless, the progression from lower right to upper left along a straight line of slope –1.0 in f_{44} vs. f_{43} space in the m-xylene experiments (e.g., Fig. 6) is also consistent with the same nature of increasing yield of CO_2^+ groups at the expense of C_2H_3O groups with increased OH exposure.

The differences between the Lawrence Berkeley National Laboratory (LBNL) study and this study are puzzling, since both of these studies used short residence times and OH and O_3 concentrations far above atmospheric levels. The OH exposures in the LBNL study (0 to 3.0×10^{12} cm^{-3} s) are comparable to those from this study (1.8×10^{11} cm^{-3} s to 2.4×10^{12} cm^{-3} s). While wall effects in the LBNL flow tube could be influencing their results, as discussed in the previous section for the flow tube of

George and Abbatt (2010), it appears more likely that the differences in the AMSs used in the two studies or in the calculations of f_{44} and f_{43} are responsible.

In Fig. 7, note that the line representing the LBNL result is roughly parallel to the results from this study. This parallel shift could occur if the AMS used in the LBNL study were more efficient at fragmenting the OA organics into *m/z* 43 and *m/z* 44. It could also occur if the calculation of the OA mass concentration was different from the calculation used in this study. In fact, using the fragmentation table that is commonly applied to the atmosphere for our laboratory results yields a total OA mass concentration that is 25% less than the one we used. As a result, our f_{44} and f_{43} values would shift to coincide with the LBNL results. Until there is consistency in the methods of AMS operation and mass calculation, we cannot compare these results from different studies with much certainty.

4 Conclusions

In the first paper on the Potential Aerosol Mass method, we showed that the yields of OA from individual organic precursor gases were similar to those obtained in large environmental chambers (Kang et al., 2007). In this study, we show that the extent of OA oxidation appears to be similar to that observed in the atmosphere and greater than that observed in large environmental chambers and laboratory flow tubes. The similarities between the OA in the atmosphere and the PAM chamber include the following properties: mass spectra; f_{44} of 0.10 to 0.18 and thus O:C of 0.4 to 0.8; f_{44}/f_{43} of 0.4 to 3.2; and points on an f_{44} vs. f_{43} plot that are close to or within the triangle containing results from atmospheric measurements. This statement is valid only for the few organic precursor gases α-pinene, *m*-xylene, and *p*-xylene, and a mixture of them. More studies will be necessary to see how universal these results are.

This study highlights the value of small flow-through photo-oxidation chambers, like the PAM chamber, for examining the atmospheric oxidation of OA. While there is some evidence from another study that the OH levels are as important as the OH exposure,

so that the slower oxidation of the atmosphere is different from the faster oxidation of the PAM chamber, the results from this study suggest otherwise.

A caveat in the comparisons of the results of this study from those of other atmospheric and laboratory studies is the possible differences in the operation of the AMS (in particular, oven temperature) and the calculation of the OA mass concentration. In this paper, we provide an explicit description of the calculation of the OA mass concentration. While similar descriptions or references to detailed descriptions have been provided in many published papers, they have not been provided in all. It would be very useful for future PAM-chamber studies to examine the sensitivity of f_{44} and f_{43} to oven temperature and to assumptions necessary for calculating the total OA mass concentration. To a large degree, the ambiguities in calculating the total OA mass concentration from Q-AMS results are not an issue with the high-resolution ToF-AMS instruments.

The highly linear behavior of f_{44}, which has greater contribution in LV-OOA, and f_{43}, which has greater contribution in SV-OOA, is clearly observed in this study. It is surprising that both α-pinene and the xylenes have similar behavior, and it is not clear if the organics from other precursor organics would behave the same way in this PAM chamber. While the absolute values of f_{43} and f_{44} are subject to the caveats in the previous paragraph, the slopes of linear regressions for f_{44} and f_{43} vs. OH exposure and f_{44} vs. f_{43} are not. The slope of -1 on the f_{44} vs. f_{43} plot and the constancy of the sum of f_{44} and f_{43} suggest that these two masses represent essentially all of the organics in the OA as they oxidize and shift from C_2H_3O groups to CO_2^+ groups for α-pinene, m-xylene, and p-xylene.

The linear regressions of f_{44} and f_{43} measurements from some of other laboratory studies and the atmosphere have slopes quite similar to -1 on a plot of f_{44} vs. f_{43} but some of them are not. These slopes could be different for a variety of reasons. If other processes are occurring, like the preferential removal of LV-OOA by clouds or surfaces for atmospheric OA or walls in the environmental chambers, then removal of organics contributing to f_{44} will reduce f_{44} more than f_{43}, causing scatter in the plot. The slope

could also change if fresh, less oxidized organics condense on more aged SOA, thus increasing f_{43} while decreasing f_{44}, also resulting in scatter in the plot. Differences in the organic composition from the oxidation of different mixtures of precursor VOCs could also result in a different oxidation pathways, leading to different relationships between f_{44} and f_{43} (Ng et al., 2009, Fig. 6b). Likely there are many causes, especially in the atmosphere.

These conclusions suggest several lines of inquiry for future research. First, the determination of the OA mass concentration has to be standardized in a way that permits meaningful comparisons among different studies. Second, the oxidation of many other atmospheric VOCs, and indeed organics in ambient air itself, needs to be studied to see how universal this behavior is, particularly the -1 slope for f_{44} vs. f_{43} and the constancy of the sum of f_{44} and f_{43}. And third, the causes of differences in the oxidation slopes need to be identified, understood, and cataloged for importance to the real atmosphere.

References

Aiken, A. C., DeCarlo, P. F., Kroll, J. H., Worsnop, D. R., Huffman, J. A., Docherty, K. S., Ulbrich, I. M., Mohr, C., Kimmel, J. R., Sueper, D., Sun, Y., Zhang, Q., Trimborn, A., Northway, M., Ziemann, P., Canagaratna, M. R., Onasch, T. B., Alfarra, M. R., Prévôt, A. H., Dommen, J., Duplissy, J., Metzger, A., Baltensperger, U., and Jimenez, J. L.: O/C and OM/OC ratios of primary, secondary, and ambient organic aerosols with high-resolution time-of-flight aerosol mass spectrometry, Environ. Sci. Technol., 42, 4478–4485, 2008.

Alfarra, M. R., Paulsen, D., Gysel, M., Garforth, A. A., Dommen, J., Prévôt, A. S. H., Worsnop, D. R., Baltensperger, U., and Coe, H.: A mass spectrometric study of secondary organic aerosols formed from the photooxidation of anthropogenic and biogenic precursors in a reaction chamber, Atmos. Chem. Phys., 6, 5279–5293, doi:10.5194/acp-6-5279-2006, 2006.

Allan, J. D, Alfarra, M. R, Bower, K. N., Williams, P. I., Gallagher, M. W., Jimenez, J. L., Mc-Donald, A. G., Nemitz, E., Canagaratna, M. R., Jayne, J. T., Coe, H., and Worsnop, D. R.: Quantitative sampling using an Aerodyne Aerosol Mass Spectrometer. Part 2: measurements of fine particulate chemical composition in two UK Cities, J. Geophys. Res. Atmos., 108(D3), 4091, doi:4010.1029/2002JD002359, 2003.

Allan, J. D., Coe, H., Bower, K. N., Alfarra, M. R., Delia, A. E., Jimenez, J. L., Middlebrook, A. M., Drewnick, F., Onasch, T. B., Canagaratna, M. R., Jayne, J. T., and Worsnop, D. R.: Technical note: extraction of chemically resolved mass spectra from Aerodyne aerosol mass spectrometer data, Aerosol Sci., 35, 909–922, 2004.

Bahreini, R., Keywood, M. D., Ng, N. L., Varutbangkul, V., Gao, S., Flagan, R. C., Seinfeld, J. H., Worsnop, D. R., and Jimenez, J. L.: Measurements of secondary organic aerosol from oxidation of cycloalkenes, terpenes, and m-xylene using an Aerodyne aerosol mass spectrometer, Environ. Sci. Technol., 39, 5674–5688, 2005.

Baltensperger, U., Dommen, J., Alfarra, M. R., Duplissy, J., Gaeggeler, K., Metzger, A., Facchini, M. C., Decesari, S., Finessi, E., Reinnig, C., Schott, M., Warnke, J., Hoffmann, T., Klatzer, B., Puxbaum, H., Geiser, M., Savi, M., Lang, D., Kalberer, M., and Geiser, T.: Combined determination of the chemical composition and of health effects of secondary organic aerosols: the POLYSOA project, J. Aerosol Med. Pulm. Drug. Deliv., 21(1), 145–154, 2008.

Canagaratna, M. R., Jayne, J. T., Jimenez, J. L., Allan, J. D., Alfarra, M. R., Zhang, Q., Onasch, T. B., Drewnick, R., Coe, H., Middlebrook, A., Delia, A., Williams, L. R., Trimborn, A. M., Northway, M. J., DeCarlo, P. F., Kolb, C. E., Davidovits, P., and Worsnop, D. R.: Chemical and microphysical characterization of ambient aerosols with the Aerodyne aerosol mass spectrometer, Mass Spectrom. Rev., 26, 185–222, 2007.

Chan, M. N., Chan, A. W. H., Chhabra, P. S., Surratt, J. D., and Seinfeld, J. H.: Modeling of secondary organic aerosol yields from laboratory chamber data, Atmos. Chem. Phys., 9, 5669–5680, doi:10.5194/acp-9-5669-2009, 2009.

Donahue, N. M., Robinson, A. L., Stanier, C. O., and Pandis, S. N.: Coupled partitioning, dilution, and chemical aging of semivolatile organics, Environ. Sci. Technol., 40, 2635–2643, 2006.

Drewnick, F., Hings, S. S., DeCarlo, P. F., Jayne, J. T., Gonin, M., Fuhrer, K., Weimer, S., Jimenez, J. L., Demerjian, K. L., Borrmann, S., and Worsnop, D. R.: A new Time-of-Flight Aerosol Mass Spectrometer (ToF-AMS) – instrument description and first field deployment, Aerosol Sci. Tech., 39, 637–658, 2005.

SOA oxidation PAM chamber studies

E. Kang et al.

Dzepina, K., Volkamer, R. M., Madronich, S., Tulet, P., Ulbrich, I. M., Zhang, Q., Cappa, C. D., Ziemann, P. J., and Jimenez, J. L.: Evaluation of recently-proposed secondary organic aerosol models for a case study in Mexico City, Atmos. Chem. Phys., 9, 5681–5709, doi:10.5194/acp-9-5681-2009, 2009.

Faloona, I. C., Tan, D., Lesher, R. L., Hazen, N. L., Frame, C. L., Simpas, J. B., Harder, H., Martinez, M., Di Carlo, P., Ren, X., and Brune, W. H.: A laser-induced fluorescence instrument for detecting tropospheric OH and HO_2: characteristics and calibration, J. Atmos. Chem., 139–167, 2004.

Forster, P., Ramaswamy, V., Artaxo, P., Berntsen, T., Betts, R., Fahey, D. W., Haywood, J., Lean, J., Lowe, D. C., Myhre, G., Nganga, J., Prinn, R., Raga, G., Schulz, M., and Van Dorland, R.: Changes in atmospheric constituents and in radiative forcing, in: Climate Change 2007: The physical science basis. Contribution of working group I to the fourth assessment report of the Intergovernmental Panel on Climate Change, edited by: Solomon, S., Qin, D., Manning, M., Chen, Z., Marquis, M. K. B., 2007.

George, I. J. and Abbatt, J. P. D.: Chemical evolution of secondary organic aerosol from OH-initiated heterogeneous oxidation, Atmos. Chem. Phys., 10, 5551–5563, doi:10.5194/acp-10-5551-2010, 2010.

Gross, D. S., Gälli, M. E., Kalberer, M., Prévôt, A. S. H., Dommen, J., Alfarra, M. R., Duplissy, J., Gaeggeler, K., Gascho, A., Metzger, A., and Baltensperger, U.: Real-time measurement of oligomeric species in secondary organic aerosol with the aerosol time-of-flight mass spectrometer, Anal. Chem., 78, 2130–2137, 2006.

Heald, C. L., Kroll, J. H., Jimenez, J. L., Docherty, K. S., DeCarlo, P. F., Aiken, A. C., Chen, Q., Martin, S. T., Farmer, D. K., and Artaxo, P.: A simplified description of the evolution of organic aerosol composition in the atmosphere, Geophys. Res. Lett., 37, L08803, doi:10.1029/2010GL042737, 2010.

Hoyle, C. R., Myhre, G., Berntsen, T. K., and Isaksen, I. S. A.: Anthropogenic influence on SOA and the resulting radiative forcing, Atmos. Chem. Phys., 9, 2715–2728, doi:10.5194/acp-9-2715-2009, 2009.

Jang, M., Ghio, A. J., and Cao, G.: Exposure of BEAS-2B cells to secondary organic aerosol coated on magnetic nanoparticles., Chem. Res. Toxicol., 19(8), 1044–1050, 2006.

Jayne, J. T., Leard, D. C., Zhang, X., Davidovits, P., Smith, K. A., Kolb, C. E., and Worsnop, D. R.: Development of an Aerosol Mass Spectrometer for size and composition analysis of submicron particles, Aerosol. Sci. Tech., 33, 49–70, 2000.

Title Page

Abstract | Introduction

Conclusions | References

Tables | Figures

◄ | ►

Back | Close

Full Screen / Esc

Printer-friendly Version

Interactive Discussion

Jimenez, J. L., Canagaratna, M. R., Donahue, N. M., Prévôt, A. S. H., Zhang, Q., Kroll, J. H., DeCarlo, P. F., Allan, J. D., Coe, H., Ng, N. L., Aiken, A. C., Docherty, K. S., Ulbrich, I. M., Grieshop, A. P., Robinson, A. L., Duplissy, J., Smith, J. D., Wilson, K. R., Lanz, V. A., Hueglin, C., Sun, Y. L., Tian, J., Laaksonen, A., Raatikainen, R., Rautiainen, J., Vaatto-vaara, P., Ehn, M., Kulmala, M., Tomlinson, J. M., Collins, D. R., Cubison, M. J., Dun-lea, E. J., Huffman, J. A., Onasch, T. B., Alfarra, M. R., Williams, P. I., Bower, K., Kondo, K., Schneider, J., Drewnick, F., Borrmann, S., Weimer, S., Demerjian, K., Salcedo, D., Cot-trell, L., Griffin, R., Takami, A., Miyoshi, T., Hatakeyama, S., Shimono, A., Sun, J. Y., Zhang, Y. M., Dzepina, K., Kimmel, J. R., Sueper, D., Jayne, J. T., Herndon, S. C., Trim-born, A. M., Williams, L. R., Wood, E. C., Middlebrook, A. M., Kolb, C. E., Baltensperger, U., and Worsnop, D. R.: Evolution of organic aerosols in the atmosphere, Science, 326, 1525–1529, 2009.

Kanakidou, M., Seinfeld, J. H., Pandis, S. N., Barnes, I., Dentener, F. J., Facchini, M. C., Van Dingenen, R., Ervens, B., Nenes, A., Nielsen, C. J., Swietlicki, E., Putaud, J. P., Balkanski, Y., Fuzzi, S., Horth, J., Moortgat, G. K., Winterhalter, R., Myhre, C. E. L., Tsigaridis, K., Vignati, E., Stephanou, E. G., and Wilson, J.: Organic aerosol and global climate modelling: a review, Atmos. Chem. Phys., 5, 1053–1123, doi:10.5194/acp-5-1053-2005, 2005.

Kang, E., Root, M. J., Toohey, D. W., and Brune, W. H.: Introducing the concept of Potential Aerosol Mass (PAM), Atmos. Chem. Phys., 7, 5727–5744, doi:10.5194/acp-7-5727-2007, 2007.

Kroll, J. H., Ng, N. G., Murphy, S. M., Flagan, R. C., and Seinfeld, J. H.: Secondary organic aerosol formation from Isoprene photooxidation, Environ. Sci. Technol., 40, 1869–1877, 2006.

Kroll, J. H., Smith, J. D., Che, D. L., Kessler, S. H., Worsnop, D. R., and Wilson, K. R.: Mea-surement of fragmentation and functionalization pathways in the heterogeneous oxidation of oxidized organic aerosol, Phys. Chem. Chem. Phys., 11, 8005–8014, 2009.

Lambe, A. T., Zhang, J., Sage, A. M., and Donahue, N. M.: Controlled OH radical production via ozone-alkene reactions for use in aerosol aging studies, Environ. Sci. Technol., 41(7), 2357–2363, 2007.

Lanz, V. A., Alfarra, M. R., Baltensperger, U., Buchmann, B., Hueglin, C., and Prévôt, A. S. H.: Source apportionment of submicron organic aerosols at an urban site by factor analytical modelling of aerosol mass spectra, Atmos. Chem. Phys., 7, 1503–1522, doi:10.5194/acp-7-1503-2007, 2007.

Title Page

Abstract | Introduction

Conclusions | References

Tables | Figures

◄◄ | ►►

◄ | ►

Back | Close

Full Screen / Esc

Printer-friendly Version

Interactive Discussion

Matsunaga, A. and Ziemann, P. J.: Gas-wall partitioning of organic compounds in a Teflon film chamber and potential effects on reaction product and aerosol yield measurements, Aerosol. Sci. Tech., 44(10), 881–892, 2010.

McGraw, R. and Saunders, J. H.: A condensation feedback mechanism for oscillatory nucleation and growth, Aerosol. Sci. Tech., 3, 367–380, 1984.

Myhre, G., Berglen, T. F., Johnsrud, M., Hoyle, C. R., Berntsen, T. K., Christopher, S. A., Fahey, D. W., Isaksen, I. S. A., Jones, T. A., Kahn, R. A., Loeb, N., Quinn, P., Remer, L., Schwarz, J. P., and Yttri, K. E.: Modelled radiative forcing of the direct aerosol effect with multi-observation evaluation, Atmos. Chem. Phys., 9, 1365–1392, doi:10.5194/acp-9-1365-2009, 2009.

Nel, A.: Air pollution-related illness: effects of particles, Science, 308, 804–806, 2005.

Ng, N. L., Canagaratna, M. R., Zhang, Q., Jimenez, J. L., Tian, J., Ulbrich, I. M., Kroll, J. H., Docherty, K. S., Chhabra, P. S., Bahreini, R., Murphy, S. M., Seinfeld, J. H., Hildebrandt, L., Donahue, N. M., DeCarlo, P. F., Lanz, V. A., Prévôt, A. S. H., Dinar, E., Rudich, Y., and Worsnop, D. R.: Organic aerosol components observed in Northern Hemispheric datasets from Aerosol Mass Spectrometry, Atmos. Chem. Phys., 10, 4625–4641, doi:10.5194/acp-10-4625-2010, 2010.

NIST chemical Kinetics Database, Version 7.0, 2000.

Odum, J., Hoffmann, T., Bowman, F., Collins, D., Flagan, R., and Seinfeld, J. H.: Gas/particle partitioning and secondary organic aerosol yields, Environ. Sci. Technol., 30, 2580–2585, 1996.

Root, M. J.: Determining the major oxidants in an environmental chamber. MS Thesis, The Pennsylvania State University, 2007.

Rudich, Y., Donahue, N. M., and Mentel, T. F.: Aging of organic aerosol: bridging the gap between laboratory and field studies, Annu. Rev. Phys. Chem., 58, 321–352, 2007.

Shilling, J. E., Chen, Q., King, S. M., Rosenoern, T., Kroll, J. H., Worsnop, D. R., DeCarlo, P. F., Aiken, A. C., Sueper, D., Jimenez, J. L., and Martin, S. T.: Loading-dependent elemental composition of α-pinene SOA particles, Atmos. Chem. Phys., 9, 771–782, doi:10.5194/acp-9-771-2009, 2009.

Surratt, J. D., Murphy, S. M., Kroll, J. H., Ng, N. L., Hildebrandt, L., Sorooshian, A., Szmigielski, R., Vermeylen, R., Maenhaut, W., Claeys, M., Flagan, R. C., and Seinfeld, J. H.: Chemical composition of secondary organic aerosol formed from the photooxidation of Isoprene, J. Phys. Chem. A., 110, 9665–9690, 2006.

Ulbrich, I. M., Canagaratna, M. R., Zhang, Q., Worsnop, D. R., and Jimenez, J. L.: Interpretation of organic components from Positive Matrix Factorization of aerosol mass spectrometric data, Atmos. Chem. Phys., 9, 2891–2918, doi:10.5194/acp-9-2891-2009, 2009.

Volkamer, R., Jimenz, J. L., Martini, F. S., Dzepina, K., Zhang, Q., Salcedo, D., Molina, L. T., Worsnop, D. R., and Molina, M. J.: Secondary organic aerosol formation from anthropogenic air pollution: rapid and higher than expected, J. Geophys. Res., 33, doi:10.1029/2006GL026899, 2006.

Warren, B., Song, C., and Cocker III, D. R.: Light intensity and light source influence on secondary organic aerosol formation for the m-xylene/NO$_x$ photooxidation system, Environ. Sci. Technol., 42, 5461–5466, 2008.

Zhang, Q., Alfarra, M. R., Worshop, D. R., Allan, J. D., Coe, H., Canagaratna, M. R., and Jimenez, J. L.: Deconvolution and quantification of hydrocarbon-like and oxygenated organic aerosols based on Aerosol Mass Spectrometry, Environ. Sci. Technol., 39, 4938–4952, 2005.

Zhang, Q., Jimenez, J. L., Canagaratna, M. R., Allan, J. D., Coe, H., Ulbrich, I., Alfarra, M. R., Takami, A., Middlebrook, A. M., Sun, Y. L., Dzepina, K., Dunlea, E., Docherty, K., DeCarlo, P. F., Salcedo, D., Onasch, T., Jayne, J. T., Miyoshi, T., Shimono, A., Hatakeyama, S., Takegawa, N., Kondo, Y., Schneider, J., Drewnick, F., Borrmann, S., Weimer, S., Demerjian, K., Williams, P., Bower, K., Bahreini, R., Cottrell, L., Griffin, R. J., Rautiainen, J., Sun, J. Y., Zhang, Y. M., and Worsnop, D. R.: Ubiquity and dominance of oxygenated species in organic aerosols in anthropogenically-influenced Northern Hemisphere midlatitudes, Geophys. Res. Lett., 34, L13801, doi:10.1029/2007GL029979, 2007.

Table 1. Experimental conditions of OH exposures and SOA concentrations for various conditions. SOA concentration was measured by a TEOM.

VOCs	ΔHC (ppbv)	OH (pptv)	OH exposure (molecules cm^{-3} s)	SOA concentration (μg/m^3)
α-pinene	7	259	1.46×10^{12}	11.8±5.09
	19	259	1.41×10^{12}	22.3±5.32
	33	259	1.36×10^{12}	61.8±7.08
	48	259	1.31×10^{12}	83.0±8.38
	57	259	1.29×10^{12}	150±13.1
	79	259	1.24×10^{12}	216±18.2
	35	63	2.83×10^{11}	114±10.5
	35	156	7.76×10^{11}	110±10.2
	35	259	1.32×10^{12}	94.5±9.14
	35	428	2.27×10^{12}	94.0±9.11
m-xylene	87	259	1.23×10^{12}	16.3±5.17
	160	259	1.14×10^{12}	67.3±7.40
	362	259	8.89×10^{11}	172±14.8
	426	259	8.33×10^{11}	271±22.5
	150	72	2.38×10^{11}	66.3±7.34
	150	156	6.18×10^{11}	63.4±7.17
	150	269	1.18×10^{12}	53.0±6.59
	150	394	1.87×10^{12}	52.4±6.56
	150	480	2.40×10^{12}	56.6±6.78
p-xylene	141	259	1.15×10^{12}	17.9±5.20
	204	259	1.07×10^{12}	50.6±6.47
	263	259	9.98×10^{11}	86.6±8.58
	371	259	8.92×10^{11}	245±20.5
	133	63	2.13×10^{11}	69.6±7.53
	133	138	5.66×10^{11}	61.1±7.04
	133	259	1.13×10^{12}	55.4±6.72
	133	334	1.57×10^{12}	52.2±6.55
A mixture (α-pinene 37 ppbv,		58	1.80×10^{11}	79.3±8.14
m-xylene 46 ppbv,		259	1.13×10^{12}	58.6±6.89
p-xylene 47 ppbv)		452	2.27×10^{12}	48.3±6.35

ACPD

10, 24053–24089, 2010

SOA oxidation PAM chamber studies

E. Kang et al.

Title Page

Abstract | Introduction

Conclusions | References

Tables | Figures

◄◄ | ►►

◄ | ►

Back | Close

Full Screen / Esc

Printer-friendly Version

Interactive Discussion

Table 2. The changes to Allan et al. (2004) fragmentation table used in this analysis.

m/z	Allan et al. (2004)	This analysis (range)
14	–	$(3.5\text{–}4.5)\times\text{frag}_{\text{organic}}$ [13][a]
16	$0.04\times\text{frag}_{\text{organic}}$[18]	$(0.18\text{–}0.25)\times\text{frag}_{\text{organic}}$ [44]
17	$0.25\times\text{frag}_{\text{organic}}$[18]	$(0.31\text{–}0.45)\times\text{frag}_{\text{organic}}$ [44]
18	$1.0\times\text{frag}_{\text{organic}}$ [44]	$(0.8\text{–}1.04)\times\text{frag}_{\text{organic}}$ [44]
19	$0.00128\times\text{frag}_{\text{organic}}$ [18]	$19-\text{frag}_{\text{water}}$[19]$-\text{frag}_{\text{air}}$ [19]
20	$0.002\times\text{frag}_{\text{organic}}$ [18]	$(0.002\text{–}0.005)\times\text{frag}_{\text{organic}}$ [44]
21	–	21
22	–	22
28	–	$(0.6\text{–}0.7)\times\text{frag}_{\text{organic}}$ [43] or $(0.8\text{–}0.9)\times\text{frag}_{\text{organic}}$ [44]
30	$0.022\times\text{frag}_{\text{organic}}$ [29]	$(0.18\text{–}0.23)\times\text{frag}_{\text{organic}}$ [29]
31	–	31
33	–	33
36	–	36
39	–	$(0.1\text{–}0.19)\times\text{frag}_{\text{organic}}$ [43]
40	–	$40-\text{frag}_{\text{air}}$[40]
46	–	$(0.03\text{–}0.06)\times\text{frag}_{\text{organic}}$ [44]
47	–	47
48	$0.5\times\text{frag}_{\text{organic}}$ [62]	$(0.33\text{–}0.66)\times\text{frag}_{\text{organic}}$ [62]

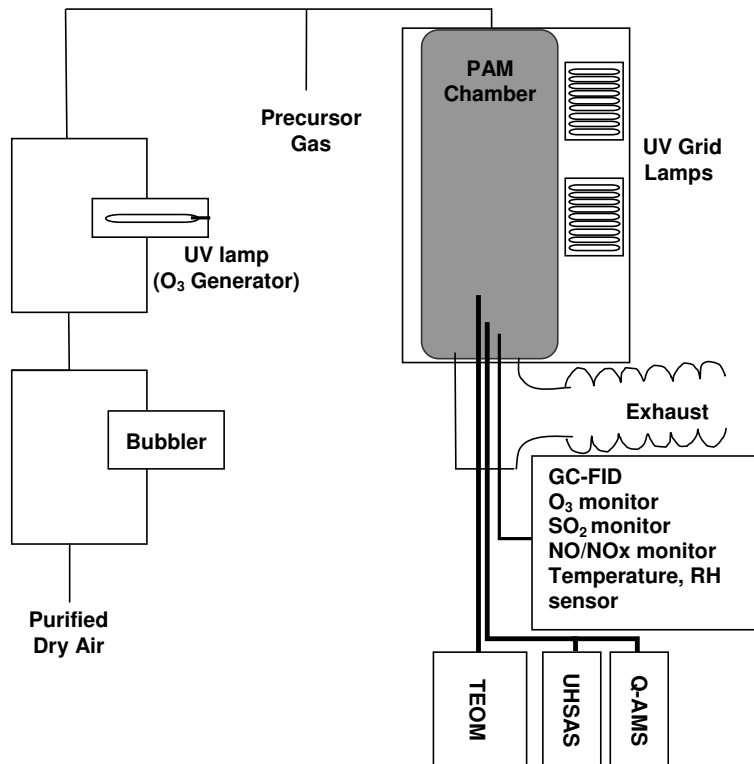[a] [m/z]: signals at the given m/z.

Fig. 1. Schematic diagram of the PAM chamber. Purified air could be humidified by passing through or around a bubbler, after which ozone and the precursor gas could be added. This gas was added uniformly across the PAM chamber cross-section; part of the flow was sampled by multiple instruments in the center of the bottom plate, while about half the flow exited through a ring surrounding the sampling tube.
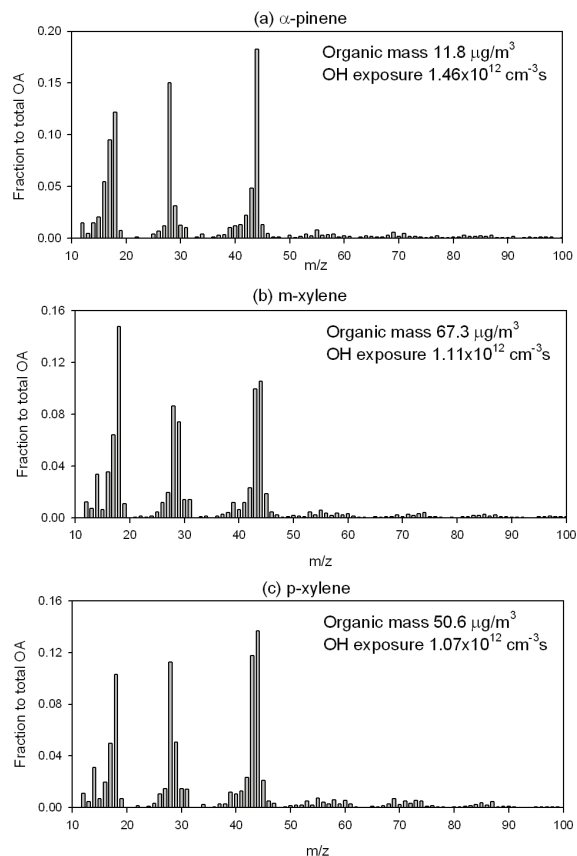
Fig. 2. Example of mass spectra of SOA for **(a)** 7 ppbv of α-pinene, **(b)** 160 ppbv of m-xylene, and **(c)** 133 ppbv of p-xylene in the PAM chamber. OH exposure was 1.53×10^{12} cm^{-3} s for no VOC addition, and resulting OH exposure for each VOCs amount are shown in the figure. All spectra are the quantitative fractional contribution to the total OA mass concentration.
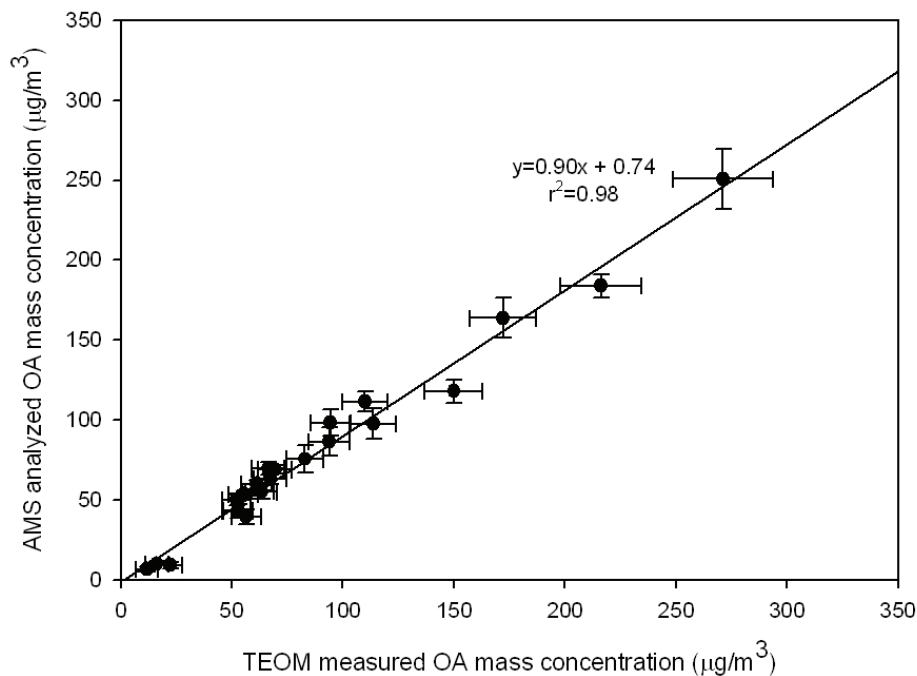
Fig. 3. AMS-analyzed OA mass concentration compared with TEOM-measured OA mass concentration. Error bars for TEOM and AMS mass concentration are the 1σ standard deviation (precision).
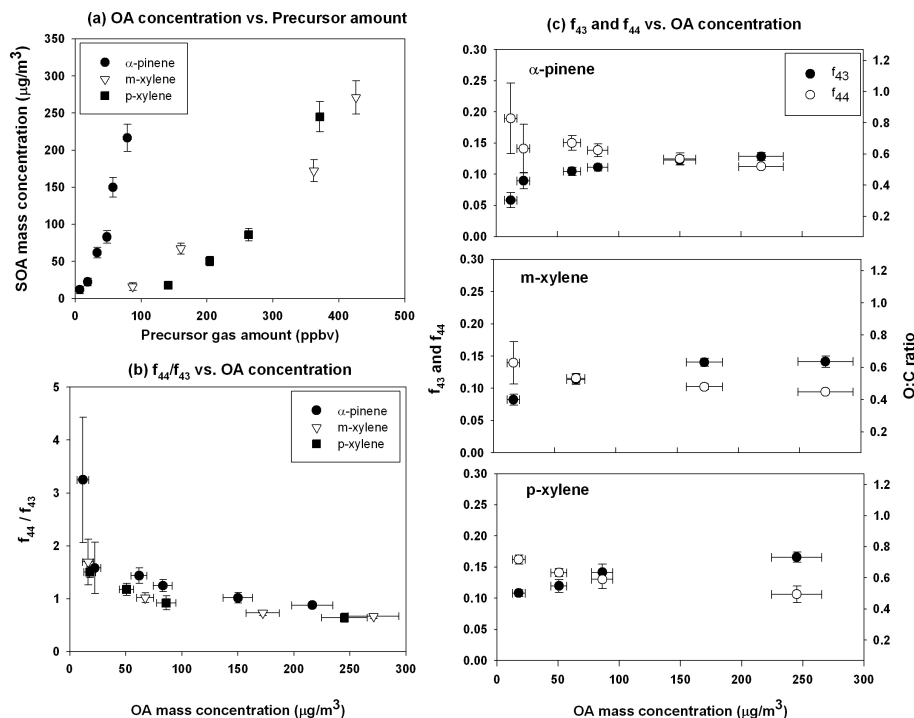
Fig. 4. SOA oxidation dependent on the OA mass concentration for α-pinene, m-xylene, and p-xylene. OH exposure was ranged between 12.4×10^{11} and 14.6×10^{11} cm^{-3} s for α-pinene, 8.3×10^{11} and 12.3×10^{11} cm^{-3} s for m-xylene, and 8.9×10^{11} and 11.5×10^{11} cm^{-3} s for p-xylene. OA mass concentration was measured by the TEOM. Error bars for SOA mass concentration, f_{43}, and f_{44} are the 1σ standard deviation (precision). **(a)** Generated OA mass concentrations vs. precursor VOCs amount. **(b)** The ratio of f_{44} to f_{43} vs. OA mass concentrations. **(c)** The values of f_{44} and f_{43} vs. OA mass concentrations. O:C ratio was calculated from f_{44} values based on Aiken et al. (2008).

Title Page

Abstract | Introduction

Conclusions | References

Tables | Figures

◀ | ▶

◀ | ▶

Back | Close

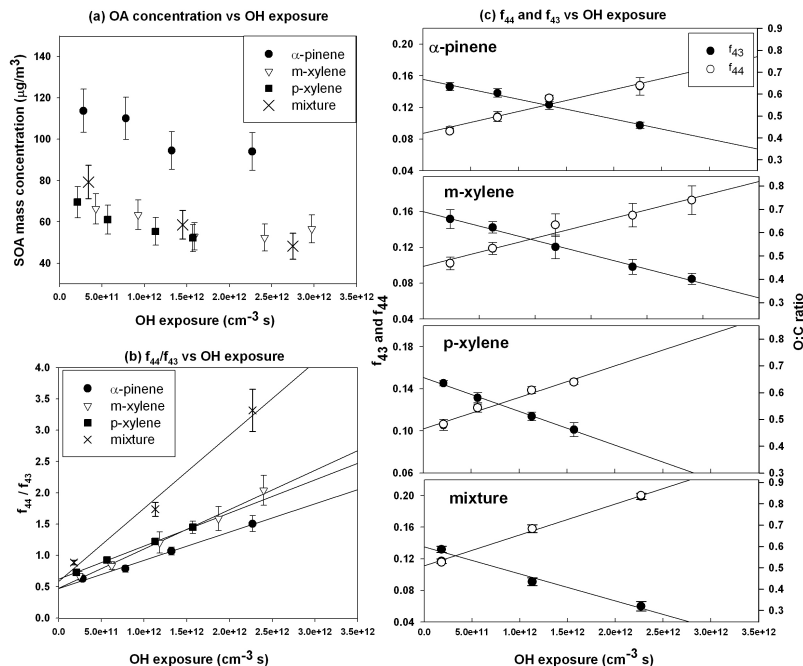Full Screen / Esc

Printer-friendly Version

Interactive Discussion

Fig. 5. SOA oxidation dependent on the OH exposure at a constant VOC amount of 35 ppbv of α-pinene, 150 ppbv of m-xylene, 133 ppbv of p-xylene, and a mixture of three (37 ppbv of α-pinene, 46 ppbv of m-xlene, 47 ppbv of p-xylene). OA mass concentration was measured by the TEOM. The error bars for OA mass concentration, f_{43}, and f_{44} are the 1σ standard deviation (precision). **(a)** OA mass concentration vs. OH exposure. **(b)** The ratio of f_{44} to f_{43} vs. OH exposure. Linear regressions of each lines are shown here; for α-pinene, slope=4.50×10^{-13}, intercept=0.47, r^2=0.99; for m-xylene, slope=6.29×10^{-13}, intercept=0.48, r^2=0.99; for p-xylene, slope=4.46×10^{-13}, intercept=0.64, r^2=0.99; and for the mixture, slope=1.17×10^{-12}, intercept=0.58, r^2=0.99. **(c)** The values of f_{43} and f_{44} vs. OH exposure. O:C ratio was calculated from f_{44} values based on Aiken et al. (2008).
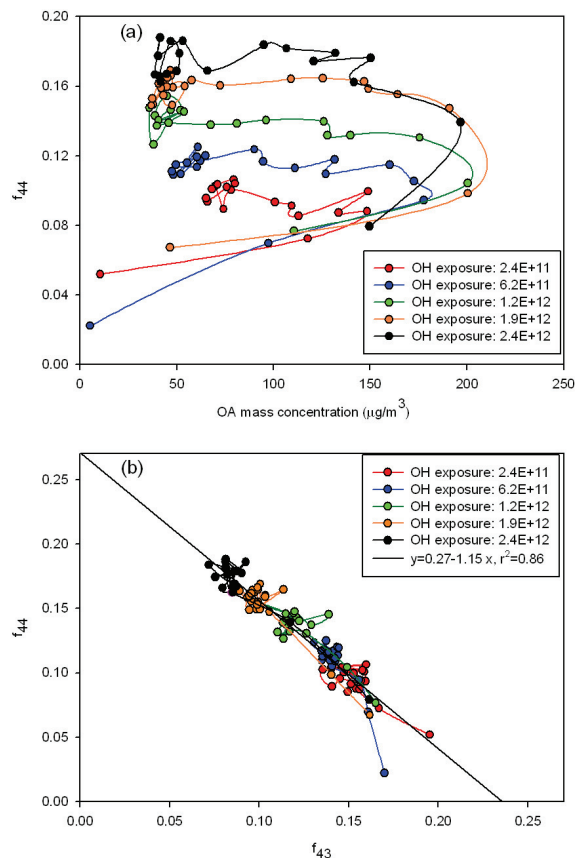
Fig. 6. Change in f_{44} and f_{43} over the course of m-xylene photo-oxidation experiment for various OH exposure conditions. **(a)** Change in f_{44} as a function of OA mass concentrations, **(b)** Change in f_{44} as a function of f_{43}. Each data point is a one-minute measurement data by the Q-AMS. The OH exposure unit is cm^{-3} s.

Full Screen / Esc

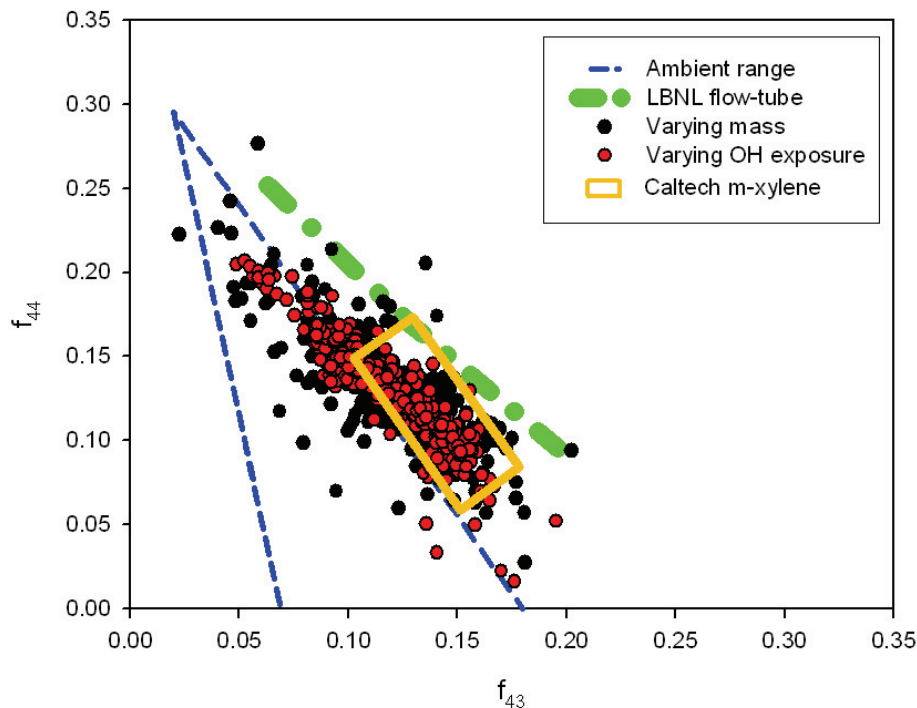Printer-friendly Version

Interactive Discussion

Fig. 7. A graph of f_{44} vs. f_{43}. Red and black circles are 1-min measurements from experiments with varying OA mass concentrations (black) and with varying OH exposure (red) in this study. Results from α-pinene photo-oxidation in the LBNL high-OH flow tube (approximated by a green dot-dashed line) and from m-xylene photo-oxidation in the Caltech environmental chamber (approximated by the orange rectangle) fall outside of the triangle (blue dashed lines) that contains atmospheric measurements (Ng et al., 2010).